Composite Structures 93 (2011) 3013–3018

Contents lists available at ScienceDirect

Composite Structures

journal homepage: www.elsevier.com/locate/compstruct

Modeling and *in situ* identification of material parameters for layered structures based on carbon nanotube arrays

J.R. Raney [a], F. Fraternali [b,c,*], A. Amendola [b], C. Daraio [a]

[a] Engineering and Applied Science, California Institute of Technology, Pasadena, CA 91125, USA
[b] Department of Civil Engineering, University of Salerno, 84084 Fisciano, SA, Italy
[c] Division of Engineering, King's College London, Strand, London WC2R 2LS, UK

ARTICLE INFO

Article history:
Available online 6 May 2011

Keywords:
Carbon nanotubes
Multilayer foams
Buckling
Mechanical properties

ABSTRACT

We test and model the mechanical response of a multilayer composite structure composed of alternating layers of aligned carbon nanotubes and copper foils under compression. We employ a bistable mass-spring model to capture the three-phase hysteretic response of the loading curve with excellent agreement with the experimental observations. An *in situ* identification procedure is proposed to quantify the material parameters corresponding to the mesoscopic scale of the structure. We refine the results using a genetic algorithm and compare the response of two different models based on three and four springs in series. The localization of deformation can be accurately captured by these simplified models, which hold promise for the design of novel materials with tailored deformation responses.

1. Introduction

Carbon nanotubes (CNTs) have been proposed for a number of applications due to their low density, high strength, and multifunctional characteristics [1]. Specifically, arrays of vertically-aligned CNTs have been proposed as field-emission electron sources [2], brushes for electrical motors [3], and fatigue-resistant foams [4]. Such arrays can be readily obtained by thermal chemical vapor deposition (CVD) with a high growth yield [5–7]. These arrays have been likened to energy-dispersive open cellular foams for their mechanical behavior under axial compression [8]. That is, they display hysteretic behavior characterized by three distinct zones: (i) linear elastic deformation for small strains, (ii) a plateau region associated with buckling for intermediate strains, and (iii) a densification regime for high strains, just as observed in typical foams [9]. The material also shows remarkable fatigue resistance when synthesized with floating catalyst techniques, able to be repeatedly compressed to large strains ($\varepsilon \geqslant 0.8$) and to still show significant recovery and dissipative effects in subsequent compressive cycles [4]. The arrays of CNTs examined in this study are efficient energy absorbers under quasistatic compression, with low bulk density (i.e., 0.1–0.3 g cm^{-3}) [10]. These characteristics suggest the applicability of these CNT arrays as possible components in advanced light-weight composites.

Additionally, it has been observed that compressed arrays of CNTs preferentially localize strain at their base, i.e., at the side nearest the growth substrate [8]. This is thought to be a result of a gradient in density along the height, increasing from the base to the top [11]. Such graded properties are known to have important effects on mechanical properties such as failure resistance and impact absorption [12], The non-uniform buckling and hysteretic behavior observed experimentally in arrays of CNTs have been recently modeled using a multi-scale mass-spring model. The model employs 1D chains of bistable springs to describe phenomena both at the microscopic and mesoscopic scales [13]. This model mathematically describes the heterogeneous, multiscale nature of aligned CNT structures, and captures the resulting sequential collapse of the material from the base upward. Here, we extend this model to the case of multilayer structures of aligned CNTs, in which multiple layers of aligned CNTs are joined by copper foil interlayers. Multilayer specimens are expected to provide superior damping performance in dynamic conditions as compared to their single layer counterparts. Multilayer structures of aligned CNTs are therefore interesting from a practical point of view, as potential light-weight components in laminar composites for energy absorption and protective systems. The multilayer structures examined in this study are constructed so that the copper interlayers between CNT arrays have a minimal influence in the overall mechanical response of the system allowing for a clearer picture of the CNT mechanics. The understanding of these systems will enable future study of more complex structures in which aligned CNTs could be partially [14] or fully [15] embedded in various polymeric matrices.

* Corresponding author at: Department of Civil Engineering, University of Salerno, 84084 Fisciano, SA, Italy. Tel.: +39 089 96 4083; fax: +39 089 96 4045.
E-mail address: f.fraternali@unisa.it (F. Fraternali).

0263-8223/$ - see front matter © 2011 Elsevier Ltd. All rights reserved.
doi:10.1016/j.compstruct.2011.04.034

Additionally, we present in this work an *in situ* identification procedure to experimentally determine the material constants that characterize the mesoscopic scale of the model proposed in [13]. To identify the material parameters, we inspect the local deformation of the CNTs through the thickness of a multilayer structure during collapse. We show that in addition to capturing the global stress and strain data obtained from experiments (as in [13]), the model can be used to capture the local deformation response at multiple length scales. To incorporate local deformation data extracted from experiments we used a high resolution CCD camera to measure local strain while the material was quasistatically compressed. This allowed a first approximation of the experimental parameters, which can be effectively used to run a successive parameter optimization procedure based on genetic algorithms (GA) [16–18], leading to highly accurate theory–experiment matching.

The rest of the paper is organized as follows: we begin by outlining the mechanical model in Section 2. This is followed, in Section 3, by an explanation of our *in situ* procedure for estimating the material characteristics that are later used as starting points for parameter optimization. In Section 4 we discuss an application of these techniques for a specific experiment based on a structure consisting of four layers of aligned CNTs separated by copper interlayers. Specifically, Section 4.1 utilizes a four spring model to approximate the sample and Section 4.2 repeats the analysis for a three spring model, revealing that the number of springs does not need to match the number of physical layers for successful theory–experiment matching. Finally, concluding remarks are given in Section 5.

2. Mechanical model

We model a multilayer CNT structure as a 1D mass-spring chain with $N+1$ lumped masses $m^0, \ldots, m^N$ connected by N nonlinear springs ($N \geqslant 2$). The mass m^0 is clamped on the bottom of the chain at position $x^0 = 0$, whereas m^N is on top at position $x^N = \ell$. The scalar quantities

$$\varepsilon^i = \frac{u^{i-1} - u^i}{h^i} \tag{1}$$

characterize the total strains of the different springs, where u^i is the axial displacement of mass m^i relative to its original position and $h^i = x^i - x^{i-1}$ (observe that spring # 1 is at the bottom, while spring # N is at the top). To allow for mechanical preconditioning, we introduce 'initial strains' $\varepsilon_0^i \geqslant 0$, and 'elastic strains' $\underline{\varepsilon}^i = \varepsilon^i - \varepsilon_0^i$ in each spring. The generic spring represents a mesoscopic dissipative element, which corresponds to the continuum limit of a lower-level (microscopic scale) chain of bistable elastic springs [13]. The constitutive equations for each spring are:

$$\sigma^i = \begin{cases} \sigma^{(a,i)} = k_0^i \underline{\varepsilon}_i / (1 - \underline{\varepsilon}^i), \\ \text{for } (\underline{\varepsilon}^i < \hat{\varepsilon}_a^i) \text{ or} \\ ((\hat{\varepsilon}_a^i < \underline{\varepsilon}^i < \varepsilon_a^i) \quad \text{and} \quad (\text{flag}^{(k-1)} \neq c)); \\ \sigma^{(d,i)} = \sigma_a^i + k_{h+}^i (\underline{\varepsilon}^i - \varepsilon_a^i), \\ \text{for } (\varepsilon_a^i \leqslant \underline{\varepsilon}^i \leqslant \hat{\varepsilon}_c^i) \quad \text{and} \quad (\text{flag}^{(k-1)} = a); \\ \sigma^{(e,i)} = \bar{\sigma}_c^i + k_{h-}^i (\underline{\varepsilon}^i - \bar{\varepsilon}_c^i), \\ \text{for } (\hat{\varepsilon}_a^i \leqslant \underline{\varepsilon}^i \leqslant \bar{\varepsilon}_c^i) \quad \text{and} \quad (\text{flag}^{(k-1)} = c); \\ \sigma^{(c,i)} = k_c^i \, (\underline{\varepsilon}^i - \varepsilon_*^i)/(1 - (\underline{\varepsilon}^i - \varepsilon_*^i)), \\ \text{for } (\underline{\varepsilon}^i > \hat{\varepsilon}_c{}^i) \text{ or} \\ \left((\bar{\varepsilon}_c^i < \underline{\varepsilon}^i < \hat{\varepsilon}_c^i) \quad \text{and} \quad (\text{flag}^{(k-1)} \neq a) \right); \end{cases} \tag{2}$$

where σ^i is the corresponding stress and, at each loading step k, it results that $\text{flag}^{(k)} = a$, if $\sigma^i = \sigma^{(a,i)}$; $\text{flag}^{(k)} = c$, if $\sigma^i = \sigma^{(c,i)}$; and $\text{flag}^{(k)} = \text{flag}^{(k-1)}$, otherwise.

The quantities k_0^i and k_c^i appearing on the right-hand side of (2) represent the slopes $d\sigma^i/d\underline{\varepsilon}^i$ at $\sigma^i = 0$ ('initial stiffnesses') of the bilateral branches $O \rightleftharpoons A_1$ (branch a) and $C_1 \rightleftharpoons C_2$ (branch b) shown in Fig. 1 (O denoting the origin of the σ^i–$\underline{\varepsilon}^i$ axes). Such branches describe the initial elastic regime and the final densification phase of the portion of the structure pertaining to the ith spring, respectively. In the same equation, the quantity k_{h+}^i represents the slope of the unilateral branch $A_1 \to C_1$, which instead describes the snap-buckling and the initial densification of such a region during loading; the quantity k_{h-}^i represents the slope of the unilateral branch $C_2 \to A_1$. The latter models the snap-back of the same region during unloading.

Concerning the stress and strain quantities appearing in (2), we remark that σ_a^i represents the stress corresponding to point A_1; $\bar{\sigma}_c^i$ represents the stress corresponding to C_2; the quantities ε_a^i, $\hat{\varepsilon}_c^i$, $\bar{\varepsilon}_a^i$ and $\hat{\varepsilon}_a^i$ indicate the strains corresponding to A_1, C_1, C_2 and A_2, respectively. The constitutive Eq. (2) can be expressed in terms of the independent parameters $k_0^i, k_c^i, k_{h+}^i, k_{h-}^i, \varepsilon_a^i, \hat{\varepsilon}_c^i$, and $\Delta\sigma^i = \sigma_a^i - \bar{\sigma}_c^i$ [13].

It is worth noting that such an equation does not allow for accumulation of permanent strain, which often affects real CNT structures (e.g., see [8]), but just for reversible (or 'transformational') plasticity [13,19]. The model could be easily generalized to capture such a phenomenon, by allowing that the snap-back of one or more springs leads to permanent deformation, and not to phase a (Fig. 1). This generalization is beyond the scope of the present work and will be addressed in future work.

3. *In situ* parameter identification

The proposed *in situ* material parameter identification procedure requires an experimental apparatus that allows the characterization of the CNT morphology alongside the load–displacement curve (e.g., by using a high resolution CCD camera as in this study, or a scanning electron microscope as in [11]). Specifically, we obtain high resolution images from the side of the structure, such that its whole height can be viewed in detail. In hard-device conditions, the order parameter of a quasi-static compression test will be the global strain ε, and the stress σ will be approximatively constant along the thickness of the structure. We suppose that ε and σ are continuously recorded during the test. Frames taken from an *in situ* video of the experiment can be used to track the local deformation of vertical portions (or segments) $\mathscr{S}^i$ of the CNT structure ($i = 1, \ldots, N$). Such regions of deformation can correspond to

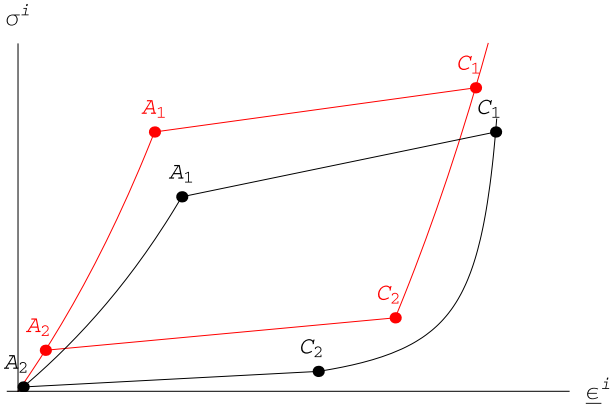

Fig. 1. Stress–strain curve of the generic spring for two different sets of material properties.

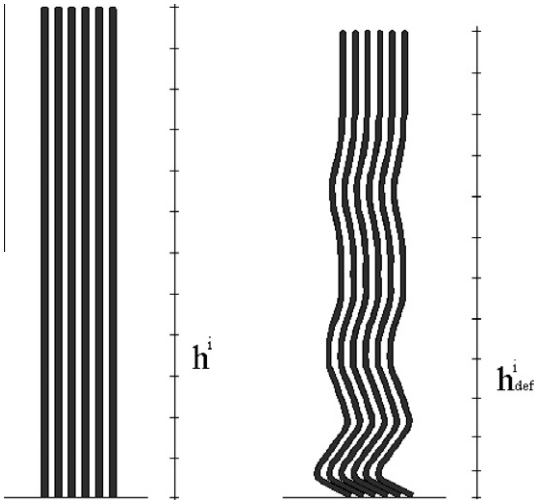

Fig. 2. Tracking of the local deformation along the axis of the carbon nanotubes.

individual CNT arrays, groups of arrays, and/or portions of individual arrays. Let h^i denote the undeformed length of $\mathscr{S}^i$, and h^i_{def} its current deformed length (Fig. 2). An approximation to the local strain ε^i of $\mathscr{S}^i$ is given by $(h^i - h^i_{def})/h^i$

$$\varepsilon^i \approx \frac{h^i - h^i_{def}}{h^i} \tag{3}$$

On using (3), and supposing $\sigma^i \approx const = \sigma$, one can easily record a local stress–strain curve σ^i vs ε^i for each of the elements $\mathscr{S}^1, \ldots, \mathscr{S}^N$.

We employ the theoretical stress–strain response described by Eq. (2) and depicted in Fig. 1 to model such experimental responses, up to the instants marking the snap-back of the CNTs from a buckled to an unbuckled state (disregarding permanent deformation effects). In particular, with reference to the generic element $\mathscr{S}^i$, we identify the point denoted by A_1 in Fig. 1 with the state immediately preceding the snap-buckling (or initial densification) of such a portion of the structure. Similarly, we identify C_1 with the state marking the beginning of the final densification phase; and C_2 with the state immediately preceding the local snap-back of the CNTs to an unbuckled state. Since the video frames are synchronized with the global stress–strain data, we obtain the local stress–strain response for any arbitrary segment. The three necessary points mentioned above are in this way determined for each segment, based on visual inspection of the video frames and the local stress–strain responses. By constraining the stress–strain response (2) to pass through the three 'experimental' points A_1, C_1 and C_2, we determine the six constitutive parameters $k^i_0, k^i_c, k^i_{h+}, \varepsilon^a_i, \hat{\varepsilon}^i_c$ and $\Delta\sigma^i$, which completely characterize the portion $OA_1C_1C_2$ of the path shown in Fig. 1.

4. Estimation of the mechanical parameters of a four-layer structure

We estimate the material parameters of a multilayer structure composed of alternating layers of vertically aligned multi-walled CNTs and copper tape, which consists of copper foil and a thin layer of adhesive on each side. The CNTs were grown by chemical vapor deposition (CVD) using ferrocene and toluene as precursors. The height of each CNT layer was approximately 1.3 mm and the area was about 25 mm^2. The average diameter of the as-grown CNTs was about 50 nm. The multilayer structure was constructed using a total of four CNT layers (labeled as layers 1–4, numbered from bottom to top). Compression tests were performed at a strain rate of 0.01 s^{-1} to a total strain ε of 0.4 using an Instron E3000. The parameter estimates hereafter refer to the first loading cycle.

4.1. Four-spring model

In the first instance, we modeled the four-layer structure as a collection of four springs, with one spring for each layer of aligned CNTs (Fig. 3). The theoretical stress–strain curves σ^i vs ε^i ($i = 1,\ldots,4$) obtained via the *in situ* identification procedure (Model # 1) are shown in Fig. 4. It is seen from such a figure that the largest strains occur in correspondence with spring (or layer) # 2, where the major CNT collapse was observed during the experiment (cf. Fig. 9). The same figure also shows that the stiffest layers are the topmost and the bottommost ones, and that the central layers exhibit a rather compliant response. It has been observed that the stiffness of aligned arrays of CNTs can vary, even within a particular growth substrate, and that this variation in stiffness correlates with a variation in bulk density [10]. Prior to the assembly of the four CNT layers into a unified structure, their bulk densities were separately computed (by measuring the mass and dividing it by the volume). It was found that the bulk densities for the middle two layers were less than those for the top and bottom layers. Thus the increased stiffness of the top and bottom layers is explained by their higher bulk densities, in accordance with previous observations. The correlation between bulk density and stiffness is not perfect, with layer 2 showing more deformation than layer 3 despite a somewhat higher density.

Fig. 5 shows a comparison between the overall σ vs ε response predicted by Model # 1 and the corresponding experimental response. The theoretical response was determined on the basis of the local stress–strain curves shown in Fig. 4, and a time-integration procedure based on the dynamical relaxation of the discrete equilibrium problem [13]. Such a procedure describes the evolution of the system during the examined experiment through two different time scales. An external time ('macro' steps) rules the quasistatic (slow) evolution of the applied deformation history, while an internal time ('meso' steps) rules the (viscous) dynamics of the microstructure rearrangements occurring at the mesoscopic level during the macro steps. The latter are induced by the 'plastic snaps' of the individual springs and determine the macroscopic hysteresis of the system [13].

Since we examined loading from the pristine state, we assumed $\varepsilon^i_0 = 0$ in each spring (no preconditioning). The fitness performance f of such a model was measured through the maximum norm of the

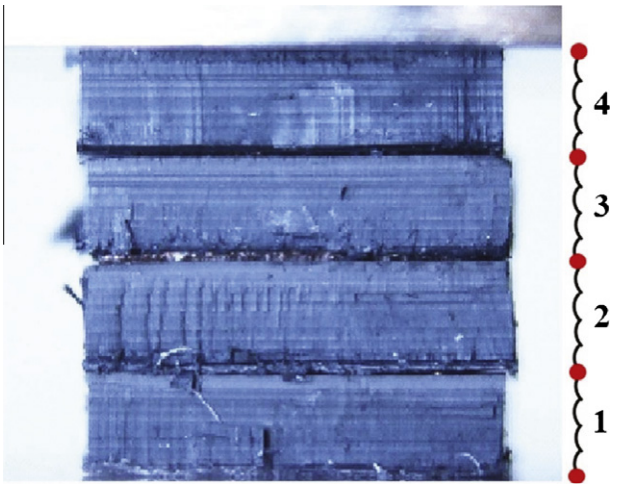

Fig. 3. A four spring scheme, in which each spring represents exactly one CNT layer, is used for Models # 1 and # 2.

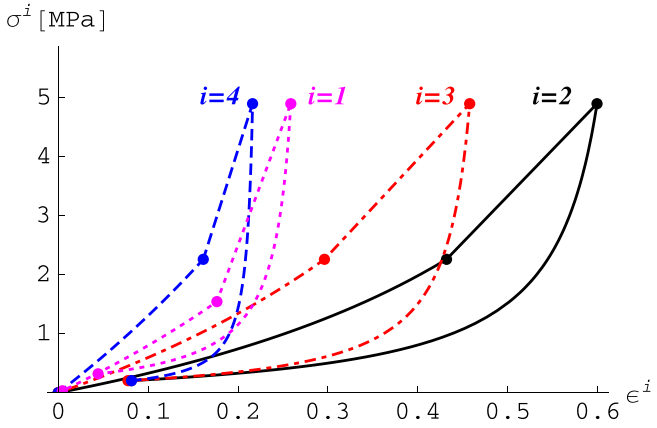

Fig. 4. *In situ* identification of the stress–strain curves of the four springs forming Model # 1.

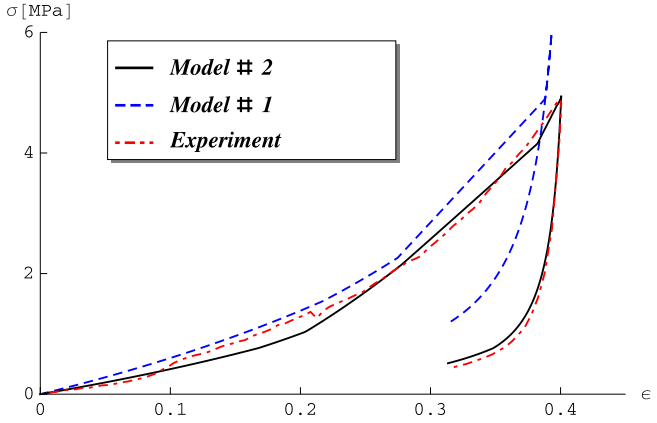

Fig. 5. Comparison between the overall stress–strain curves predicted by Models # 1 and # 2, and the recorded experimental response.

difference between the overall predicted and experimental stress–strain curves (up to the first snap-back point), obtaining $f = 1.19$ MPa. We observe in Fig. 5 agreement between Model # 1 and the experimental response, with major deviations occurring for the largest strain values ($\varepsilon \geqslant 0.3$). We were able to significantly improve the theory–experiment matching by running a GA fitting procedure. More specifically, we employed the Breeder Genetic Algorithm (BGA) presented in [18], which has been successfully used as a parameter identification tool in previous works dealing with the constitutive modeling of CNT foams [13], granular protectors [20] and soft biological tissues [21]. BGAs differ from other available GAs due to their selection mechanism, which mimics animal breeding and selects only from among the best elements of the current population (in most other GAs, selection is instead stochastic and meant to mimic Darwinian evolution). Such a feature ('truncation' selection scheme) improves the ability of BGAs when dealing with large search spaces, as compared to standard GAs (cf., e.g., [17]). For the present and the following fitting procedures, we employed a population size of 50 'individuals' (candidate solutions); a truncation rate of 15%; extended intermediate recombination [17]; and a mutation rate of 50%. We let the BGA run up to 600 generations and included in the first generation an individual with genes corresponding to the material parameters of the *in situ* identified model (Model # 1, in the present case). The BGA optimization of Model # 1 led to an improved model (Model # 2), with fitting performance $f = 0.13$ MPa. The plots shown in Fig. 5 highlight a rather good agreement between Model # 2 and the experimental response. The material parameters of Models # 1 and # 2 are provided in Table 1.

Table 1
Material constants of Models # 1 and # 2.

Model # 1 ($f = 1.19$ MPa)			
Spring	k_0^i (MPa)	k_c^i/k_0^i	k_{h+}^i/k_0^i
4	11.76	0.003	4.09
3	5.38	0.026	3.04
2	2.98	0.092	5.30
1	7.21	0.014	5.66
	ε_a^i	$\hat{\varepsilon}_c{}^i$	$\Delta\sigma^i/\sigma_a^i$
4	0.16	0.21	−0.91
3	0.30	0.43	−0.91
2	0.43	0.54	−0.91
1	0.18	0.22	−0.79
Model # 2 ($f = 0.13$ MPa)			
Spring	k_0^i (MPa)	k_c^i/k_0^i	k_{h+}^i/k_0^i
4	8.82	0.008	3.20
3	3.83	0.009	3.20
2	2.23	0.033	5.32
1	3.96	0.007	*5.70*
	ε_a^i	$\hat{\varepsilon}_c{}^i$	$\Delta\sigma^i/\sigma_a^i$
4	0.11	0.17	−0.87
3	0.36	0.52	−0.98
2	0.32	0.59	−0.98
1	0.16	0.16	−0.94

4.2. Three-spring model

As previously mentioned, the largest deformation of the CNT structure collapse was observed in experiments at the bottom of layer # 2. At the same time, the remaining portions of the multilayer structure underwent smaller deformations (cf. Fig. 9). Within an individual layer of aligned CNTs under compression, buckling begins on the side nearest the substrate, resulting in the localization of strain in this region [8,11]. Specifically, with the detail provided by scanning electron microscope as in [11], it was observed that, apart from the buckling taking place at the base of the aligned CNTs, the rest of the structure remains undeformed. That is, this would correspond to a model of compression in which all springs except one remain of nearly constant length with only one experiencing a large deformation. To design a model that would capture more closely the experimental observations, we constructed a three-spring model in which one spring was placed in correspondence with the heavily buckled region, and two other springs modeled the behavior of the remaining portions of the material below and above the deformed region (Fig. 6). Specifically, we considered a model in which the topmost spring (spring # 3) corresponds to the union of layers # 4 and # 3 plus a portion of layer # 2 (total height $h^3 = 3.24$ mm); the mid spring (spring # 2) corresponds to the remaining portion of layer # 2 ($h^2 = 0.68$ mm), in which maximum deformation was observed experimentally; and the bottom spring (spring # 1) corresponds to layer # 1 ($h^1 = 1.24$ mm).

The theoretical stress–strain curves obtained for the single springs through the *in situ* identification procedure (Model # 3) are shown in Fig. 7. It is worth noting that such stress–strain curves capture the deformation mechanism described above, with very large strains in correspondence with spring #2 (up to almost 90%), and stiffer responses in correspondence with springs #1 and #3.

Fig. 8 shows a good agreement between the overall σ vs ε response predicted by Model # 3 and the corresponding experimental response, with fitting performance $f = 1.15$ MPa. In the present

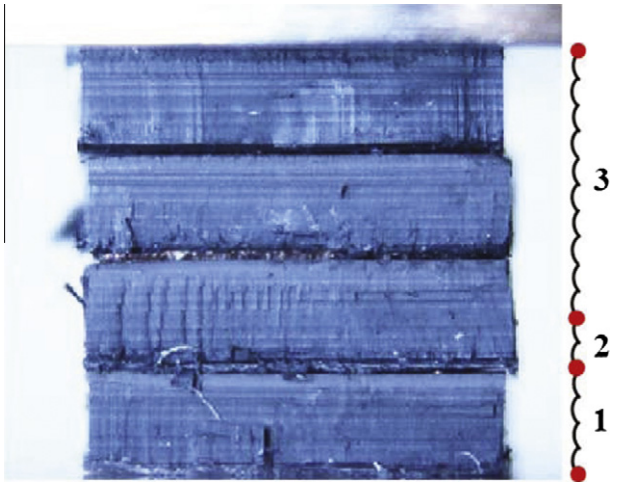

Fig. 6. A three spring scheme is used for Models # 3 and # 4.

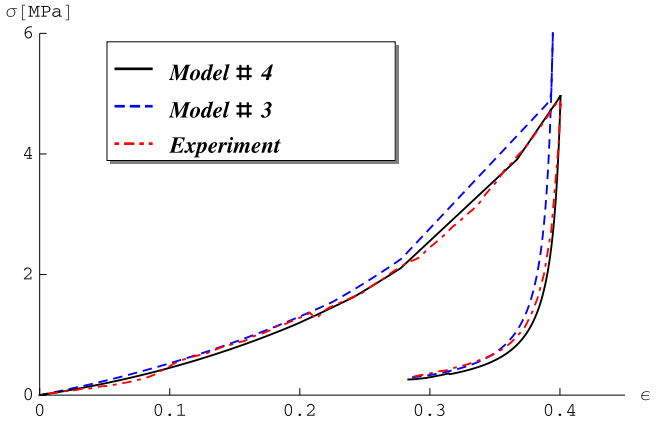

Fig. 8. Comparison between the overall stress–strain curves predicted by Models # 3 and # 4, and the recorded experimental response.

case, most of the theory–experiment deviation is localized in a very narrow region corresponding to the final portion of the densification regime ($\varepsilon \geqslant 0.35$). A BGA optimization of Model # 3 led to the response denoted as Model # 4 in Fig. 8, which shows an excellent agreement with the experimental one and fitting performance $f = 0.09$ MPa. The material parameters of Models # 3 and # 4 are provided in Table 2, while selected frames from the videos for the experiment and the response of Model # 4 are shown in Fig. 9.

Upon comparison of the optimized 4 spring and 3 spring models (i.e., Models # 2 and # 4, respectively) it is clear that the fitness performance is not driven by the number of springs so much as it is driven by the extent to which the springs correspond to the distinct behavior of the portions of the physical structure. From the experimental video, it is clear the this particular structure consists of a thin soft region surrounded by two thicker firm regions. The fitness performance of Model # 4 is superior to that of Model # 2 even though the former consists of fewer springs exactly because its springs more closely match the firm-soft-firm arrangement of the sample in question. Thus a careful viewing of the experimental recording allows one to quickly choose an appropriate, though not necessarily optimal, model. A model with a much larger number of springs could certainly be utilized, with the only limitation being the resolution of the video recording. Though this approach could be used to capture even more of the subtlety of the heterogeneous collapse of the structure, and thereby to obtain improved fitting performance, the computational time would rapidly increase. The better approach is to find the model with the minimum number of springs that provides a 'good enough' agreement with experiment, as with our three spring models in this case.

Table 2
Material constants of Models #3 and # 4.

Model # 3 ($f = 1.15$ MPa)			
Spring	k_0^i (MPa)	k_c^i/k_0^i	k_{h+}^i/k_0^i
3	7.71	0.004	3.02
2	1.09	0.081	10.60
1	7.15	0.003	6.53
	ε_a^i	$\hat{\varepsilon_c}^i$	$\Delta\sigma^i/\sigma_a^i$
3	0.23	0.33	−0.91
2	0.67	0.88	−0.91
1	0.18	0.24	−0.79
Model # 4 ($f = 0.09$ MPa)			
Spring	k_0^i (MPa)	k_c^i/k_0^i	k_{h+}^i/k_0^i
3	7.69	0.005	3.02
2	0.69	0.056	10.6
1	8.00	0.003	6.52
	ε_a^i	$\hat{\varepsilon_c}^i$	$\Delta\sigma^i/\sigma_a^i$
3	0.21	0.33	−0.87
2	0.63	0.98	−0.86
1	0.17	0.22	−0.82

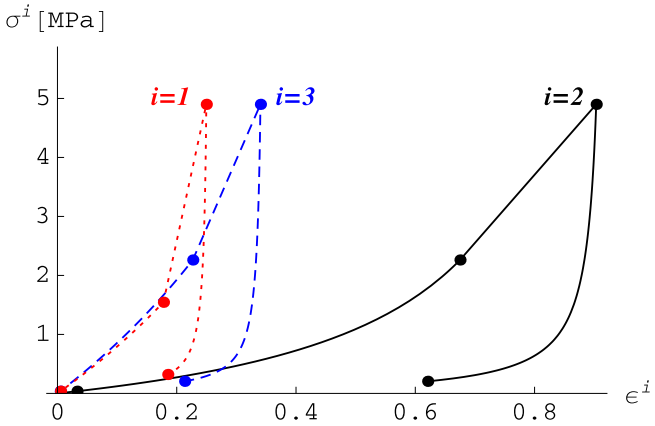

Fig. 7. *In situ* identification of the stress–strain curves of the three springs forming Model # 3.

The mechanical response of CNT arrays can vary dramatically between different growth processes. More work must be done to understand how this mechanical response depends on measurable physical characteristics (e.g., bulk density). Until this relationship is understood in detail, it is not possible to use the model for accurate experimental predictions.

5. Concluding remarks

We have presented in this work an *in situ* identification procedure for the mesoscopic mass-spring model of carbon nanotube foams recently proposed in [13]. The given procedure allows one to obtain the mechanical properties of the different springs forming such a model, through experimental characterization of local deformation of the aligned CNTs alongside a given load–displacement curve. We applied the model to characterize the mechanical reponse of a four-layer CNT structure, tracking the local deformation of the layers under compression.

The presented results show that the given identification procedure is able to produce a first approximation of the experimental

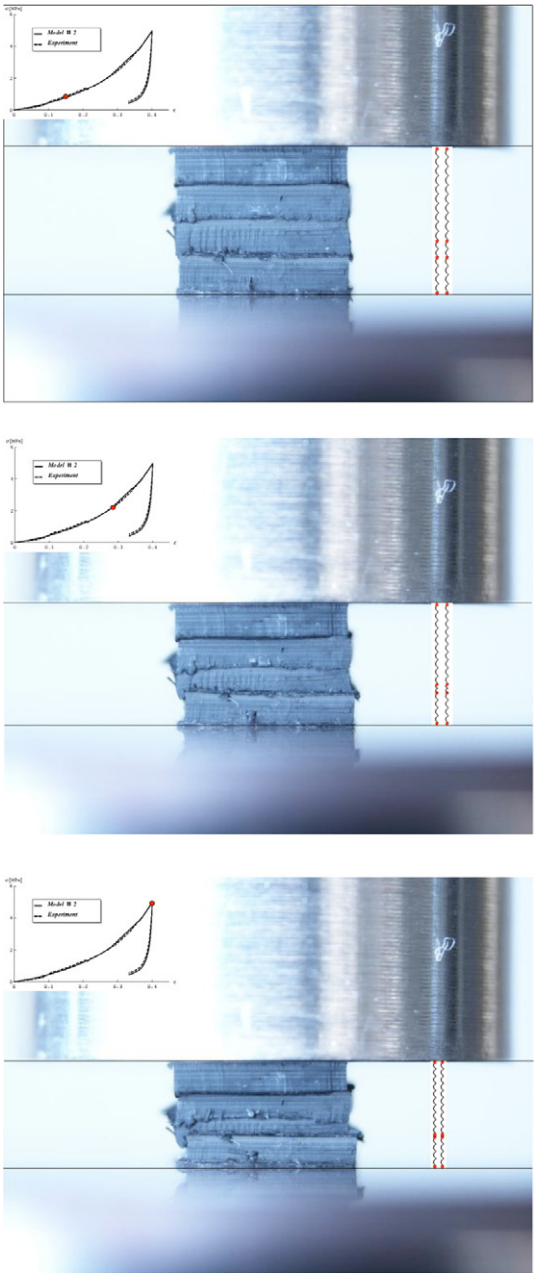

Fig. 9. Comparison between frames from the videos for the experiment and the response of Model # 4, for different values of the overall strain ε.

response, capturing its main features and reproducing the localization of the buckling deformation. This approximation can be usefully refined through a successive GA optimization of material parameters [13]. We found that a suitable choice of the fitting model (number and localization of the springs) significantly improves the theory–experiment matching.

Additionally, we have extended the work proposed in [13], which was limited to a single array of aligned CNTs, to the case of multilayer composites based on alternating layers of aligned CNTs and copper foils. In other experiments we have found that similar multilayer structures give superior response under impact when compared to a single CNT array. Modeling structures such as these is a necessary first step toward the construction of lightweight multilayer CNT-based laminar composites with tailored collapse and energy-dispersive properties.

A generalization of the procedure presented here to account for permanent deformation, and time dependence will be addressed in future work. Additional study of the response of CNT arrays at the microscopic scale (based on characterization of the local deformation with scanning electron microscopy) is also planned.

Acknowledgements

CD acknowledges support from the Institute for Collaborative Biotechnologies under contract W911NF-09-D-0001 with the Army Research Office. FF acknowledges the support of the University Centre for Risk Prediction and Prevention (CUGRI) in association between the Universities of Salerno and Napoli Federico II, Italy. FF also thanks the Graduate Aerospace Laboratory at the California Institute of Technology (GALCIT) for the hospitality during his visit. JRR gratefully acknowledges the U.S. Department of Defense and the Army Research Office for their support via a National Defense Science and Engineering Graduate (NDSEG) fellowship.

Appendix A. Supplementary data

Supplementary data associated with this article can be found, in the online version, at doi:10.1016/j.compstruct.2011.04.034.

References

[1] Baughman RH, Zakhidov AA, de Heer WA. Carbon nanotubes: the route toward applications. Science 2002;297(5582):787–92.
[2] de Heer WA, Chatelain A, Ugarte D. A carbon nanotube field-emission electron source. Science 1995;270(5239):1179–80.
[3] Toth G, Maklin J, Halonen N, Palosaari J, Juuti J, Jantunen H, et al. Carbon-nanotube-based electrical brush contacts. Adv Mater 2009;21(20):2054–8.
[4] Suhr J, Victor P, Ci L, Sreekala S, Zhang X, Nalamasu O, et al. Fatigue resistance of aligned carbon nanotube arrays under cyclic compression. Nat Nanotechnol 2007;2(7):417–21.
[5] Li WZ, Xie SS, Qian LX, Chang BH, Zou BS, Zhou WY, et al. Large-scale synthesis of aligned carbon nanotubes. Science 1996;274(5293):1701–3.
[6] Lee CJ, Park J, Huh Y, Lee JY. Temperature effect on the growth of carbon nanotubes using thermal chemical vapor deposition. Chem Phys Lett 2001;343(1–2):33–8.
[7] Andrews R, Jacques D, Rao AM, Derbyshire F, Qian D, Fan X, et al. Continuous production of aligned carbon nanotubes: a step closer to commercial realization. Chem Phys Lett 1999;303(5-6):467–74.
[8] Cao A, Dickrell PL, Sawyer WG, Ghasemi-Neihad MN, Ajayan PM. Super-compressible foamlike carbon nanotube films. Science 2005;310(5752):1307–10.
[9] Gibson LJ, Ashby MF. Cellular solids: structure and properties. Oxford: Pergamon Press; 1988.
[10] Raney JR, Misra A, Daraio C. Tailoring the microstructure and mechanical properties of arrays of aligned multiwall carbon nanotubes by utilizing different hydrogen concentrations during synthesis. Carbon 2011, in press. doi:10.1016/j.carbon.2011.04.066.
[11] Hutchens SB, Hall LJ, Greer JR. In situ mechanical testing reveals periodic buckle nucleation and propagation in carbon nanotube bundles. Adv Funct Mater 2010;20:2338–46.
[12] Suresh S. Graded materials for resistance to contact deformation and damage. Science 2001;292(5526):2447–51.
[13] Fraternali F, Blesgen T, Amendola A, Daraio C. Multiscale mass-spring models of carbon nanotube foams. J Mech Phys Solids 2011;59(1):89–102.
[14] Misra A, Greer JR, Daraio C. Strain rate effects in the mechanical response of polymer-anchored carbon nanotube foams. Adv Mater 2009;21(3):334–8.
[15] Garcia EJ, Hart AJ, Wardle BL, Slocum AH. Fabrication and nanocompression testing of aligned carbon-nanotube–polymer nanocomposites. Adv Mater 2007;19(16):2151–6.
[16] Holland JH. Outline for a logical theory of adaptive systems. J ACM 1962;9(3):297–314.
[17] Mühlenbein H, Schlierkamp-Voosen D. The science of breeding and its application to the Breeder Genetic Algorithm (BGA). Evol Comput 1994;1(4):335–60.
[18] De Falco I, Del Balio R, Della Cioppa, A, Tarantino E. A comparative analysis of evolutionary algorithms for function optimization. In: Proceedings of the Second Workshop on Evolutionary Computation (WEC2), Nagoya, Japan; 1996. p. 29–32.
[19] Puglisi G, Truskinovsky L. Thermodynamics of rate independent plasticity. J Mech Phys Solids 2005;53(3):655–79.
[20] Fraternali F, Porter MA, Daraio C. Optimal design of composite granular protectors. Mech Adv Mater Struct 2010;17(1):1–19.
[21] El Sayed T, Mota A, Fraternali F, Ortiz M. A variational constitutive model for soft biological tissue. J Biomech 2008;41:1458–66.